4. BALANCED WALKING RESULTS

This chapter describes the results of a series of experiments performed using the balance control approach of Chapter 3. Various parameter choices are explored to determine their importance in generating successful limit cycles and their effect on the resulting motion. Control of the human model is the primary focus of these experiments, although trials using the robo-bird model are also included to demonstrate success with a significantly different bipedal model. Sections 4.1, 4.2, and 4.3 present results obtained using each of the three choices of RVs introduced in Section 3.5. Section 4.4 examines the effectiveness of applying a torso servo to the human model.

Figure 4.1 shows a few steps from a typical balanced walk. The motion reaches a limit cycle and continues to walk in a straight line for the full 60 steps of the trial. Using the nominal open-loop control alone results in only 5 steps before the human figure falls over. The results clearly demonstrate that with suitable parameter choices, active stabilization of bipedal locomotion cycles is both possible and useful.

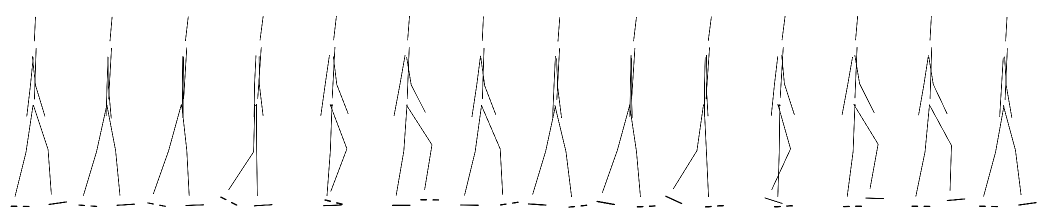

Figure 4.1 - A sequence of steps from a walking limit cycle.
Up vector-based, Q^d = [.25, 0], F-L sampling.

The motion resulting from the application of the described balance control varies significantly, depending on the choice of RVs and other parameter values. Many choices of parameter values result in a number of successful steps but eventually fall. Other values move the system onto a successful walking limit cycle. Some walks don't fall despite seemingly chaotic motion.

4.1 Up Vector Regulation Variables

The first results we show use the base PCG of Figure 3.7 and the stance hip perturbations described in Section 3.6. The RVs consist of the components of the up vector, as illustrated in Figure 3.12 (c). Torso servoing is not applied. Figure 4.2 shows a representative set of RV trajectories corresponding to successful walking trials of 60 steps. These curves are the experimentally-based equivalents of the idealized cyclic trajectories shown earlier, such as those of Figure 3.3. In three of the plots, a clear limit cycle emerges. In the fourth, the trajectory is chaotic.

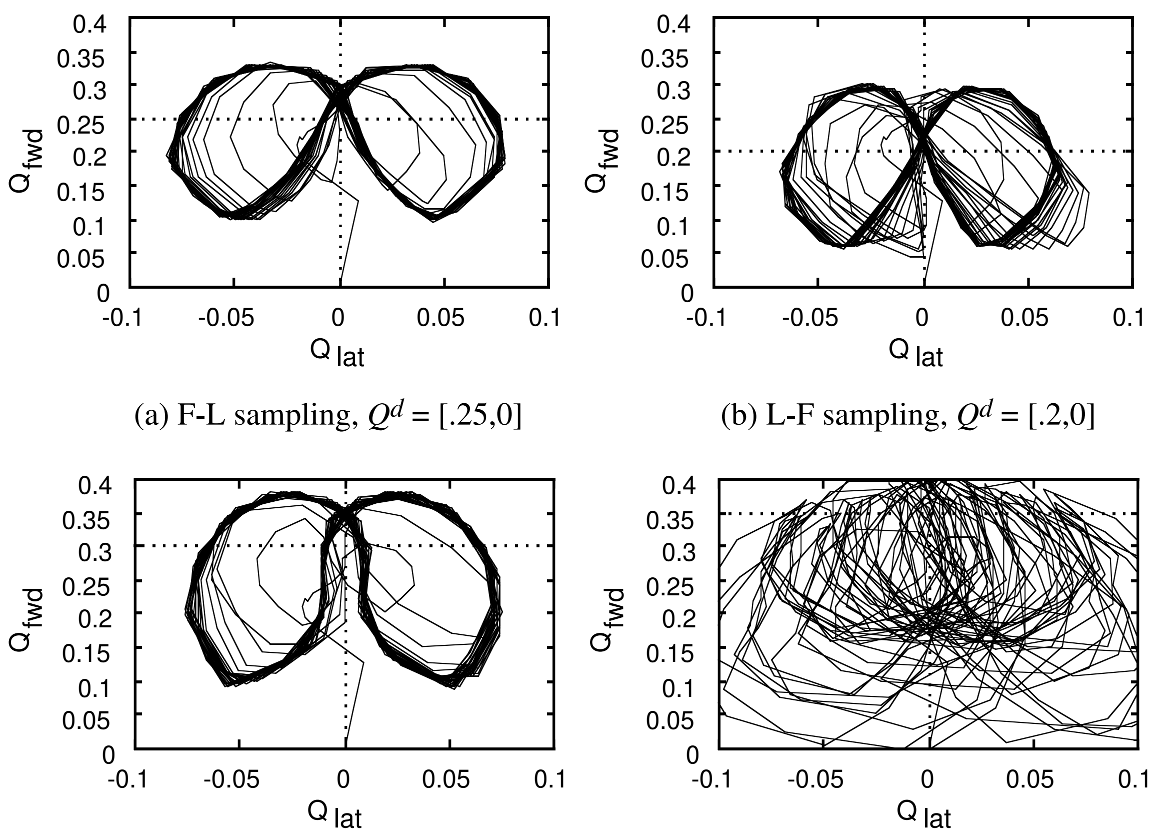

(a) F-L sampling, $Q^d = [.25,0]$

(b) L-F sampling, $Q^d = [.2,0]$

(c) SP sampling, $Q^d = [.3,0]$

(d) L-F sampling, $Q^d = [.35,0]$

Figure 4.2 - Continuous-time up-vector RV component phase diagrams

While such phase plots are useful tools for observing limit cycle behaviour in a system, they tell us relatively little about the difference between sampling strategies and/or the visual appearance of the walk.

The graphs shown in Figure 4.3 provide additional information. Graphs (a), (c) and (e) show the effect of various choices for Q^d, in particular, for the forward component of Q^d. The trials explore the useful range of this parameter by uniformly sampling a broad set of values. For each trial, the forward component of the Q^d is held constant for all steps. The lateral component is fixed at 0.0 for all trials. Walks are up to a maximum of 60 steps long and fewer than 60 successful steps indicates a fall.

The "*hip plots*" corresponding to the most successful trials for each sampling strategy are shown in Figure 4.3 (b), (d) and (f). Hip plots indicate the position and orientation of the biped's pelvis in the horizontal plane as viewed from above. This orientation information indicates the direction the biped is facing as it walks, allowing a forward motion to be easily distinguished from a lateral (sidestepping) motion. The lines on the plots are approximately 1 meter in length, significantly wider than the biped's actual hips so that their orientation can be easily seen. This affects the perceived scale of the plot, making the walks appear shorter than they actually are. The dimensions of the terrain are given in meters. The elapsed time between adjacent samples on the hip plots is approximately 0.16 seconds.

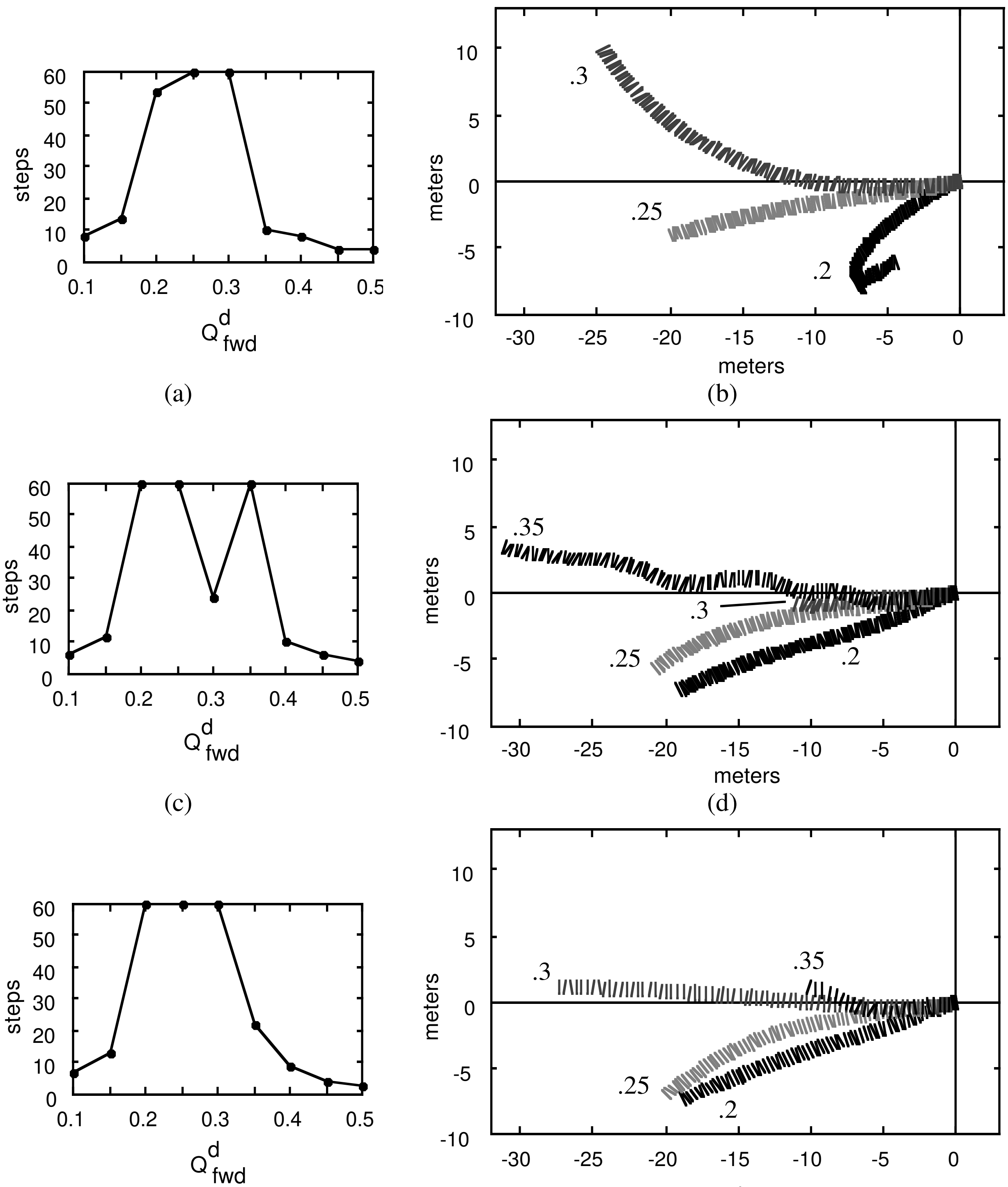

Figure 4.3 - Nominal up-vector Q^d range and corresponding hip plots for each sampling method. All trials are limited to a maximum of 60 steps. The biped initially faces left (i.e. in the -x direction).
(a) - (b) F-L sampling
(c) - (d) L-F sampling
(e) - (f) SP sampling

A number of observations can be made from these graphs and the corresponding animations:

1. Not all choices of Q^d work. Successful trials fall within a "nominal range" of Q^d which is similar across sampling strategies.
2. Choice of sampling strategy noticeably affects the appearance of the walks. Somewhat surprisingly, no one strategy is demonstrably superior.
3. Walks are not of uniform quality. Some walks initially appear stable but then fall over. Other walks appear chaotic but don't fall. Choices of Q^d toward the centre of the nominal ranges give the most consistent walks in terms of stability and appearance.
4. One walk begins moving forward, slows to a stop and then moves backwards chaotically for about 15 steps before finally falling. The fact that such a walk emerges from a base PCG designed to produce forward walking motions illustrates the potential for a broad range of useful motions with little or no change in the underlying balance mechanism.

Figure 4.4 through Figure 4.6 show the end-of-cycle components of the reduced state vector, Q_i^*, over time, for the walks of Figure 4.3 (b), (d) and (f). The sampled points are joined by lines to better visualize oscillations. The lines do not represent the continuous motion of the RV during each stride. Q^d is indicated by a dotted line.

A number of qualitative observations can be made about the behaviour of Q_i^*:

1. A startup phase is clearly evident. The number of steps required to reach a steady-state response varies from 5 to over 20, with 10 being most typical. Trials using values of Q^d in the middle of nominal range stabilize most quickly.
2. The desired value, Q^d, is not always achieved, but a limit cycle is still attained in many such cases.
3. No particular sampling strategy appears superior with respect to steady state error or rate of stabilization.

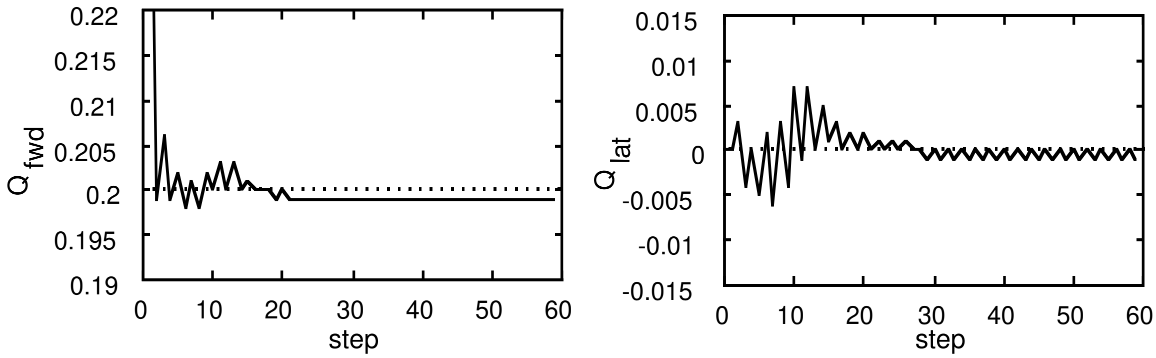

(a) forward component (b) lateral component

Figure 4.4 - Discrete RV values, Q_i^*, for L-F sampling, Q^d = [.2,0]

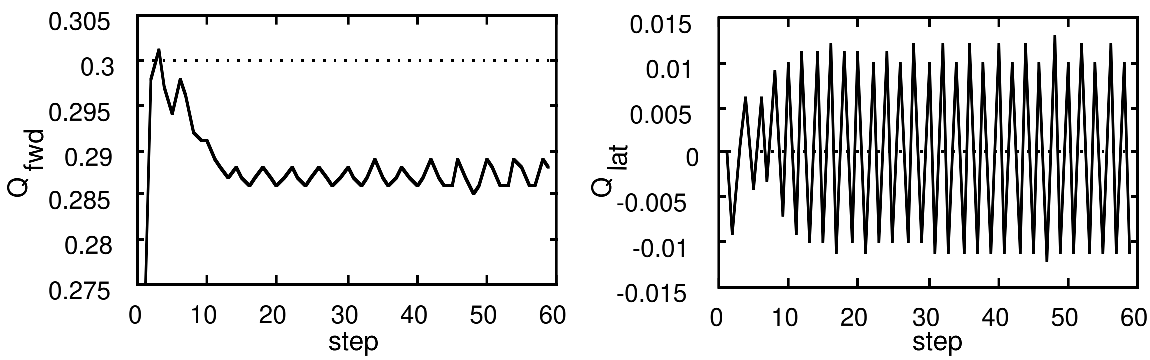

(a) forward component (b) lateral component

Figure 4.5 - Discrete RV values, Q_i^*, for SP sampling, Q^d = [.3,0]

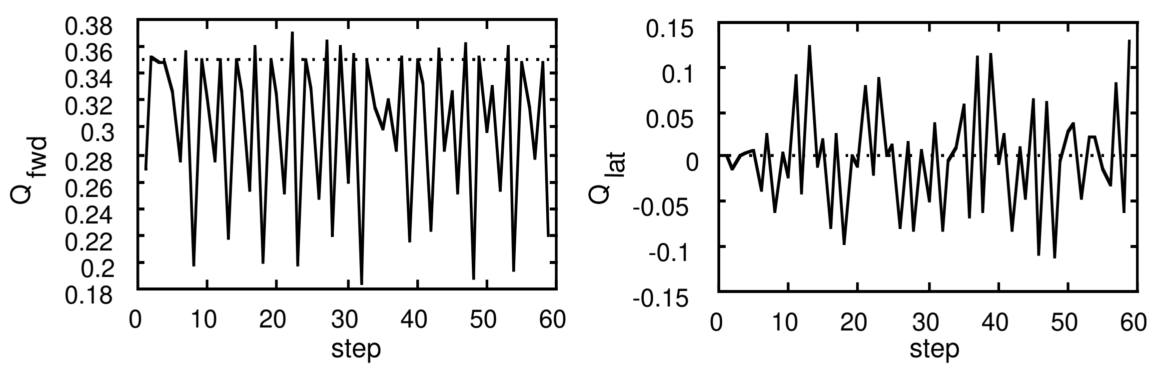

(a) forward component (b) lateral component

Figure 4.6 - Discrete RV values, Q_i^*, for L-F sampling, Q^d = [.35,0]

4. The chaotic walk (see Figure 4.6) has significantly larger error with respect to the desired RV values, Q^d, as compared to stable limit cycles (note the scale of the graph). The visual appearance of this walk is noticeably more clumsy than the other walks.
5. Generally speaking, the forward component of Q stabilizes more quickly than the lateral component and exhibits smaller variation in steady-state (e.g. Figure 4.4).
6. Q_i^* can oscillate from step to step. This is noteworthy since the overall motion should ideally have nearly identical characteristics from one step to the next.

4.1.1 Other Observations

The walks generated using the up-vector display a number of notable characteristics. First, while step length is not a regulated variable, virtually all of the walks travel a uniform distance from one step to the next. Figure 4.7 shows the step lengths over the course of a typical walk. This result is encouraging since an irregular walk would be much less appealing and a suitable remedy is not immediately obvious. This also serves as evidence that the unobservable state variables approach a limit cycle as desired.

Another characteristic of the resulting motions is that not all of the walks follow a straight line. This can be seen clearly in the hip plots of Figure 4.3. Without any form of directional control, most of the walks follow a curved path. The chaotic walk corresponding to the Q^d = [.35,0] trial of Figure 4.3 (d) follows a less regular path, weaving back and forth over the course of the trial. As we shall see in the next chapter, this can be solved by explicitly controlling the biped's direction with an additional feedback loop.

An adverse effect apparent in some of the walks is a tendency to place each stance foot directly in line with the previous in the lateral dimension as if walking a tightrope. In a few cases, this even results in the biped crossing legs slightly each step, with one leg passing through the other since such interpenetrations are not prohibited in our simulations. While the *tightrope walking* is undesirable, it is also an artifact of using the up vector RV in the lateral dimension. The lateral hip perturbations which result in this effect are chosen to maintain lateral torso uprightness. Using a different choice of RV for the lateral dimension can correct this effect, as will be demonstrated in Chapter 5.

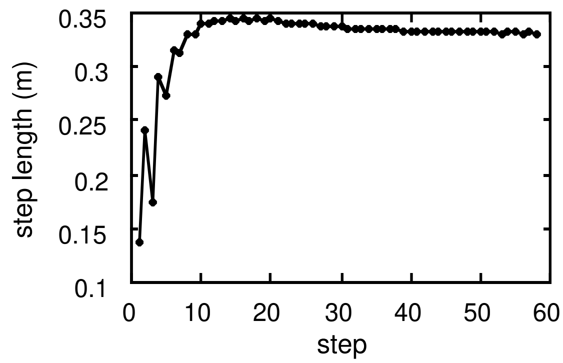

Figure 4.7 - Step length vs step number.
Q^d = [0.25,0] walk of Figure 4.3 (b)

One final characteristic of the walks is excessive front-to-back and side-to-side motion of the torso. This body motion is a result of the particular choice of control perturbations. This effect and a suitable solution will be discussed in Section 4.4.

4.2 Swing-COM Regulation Variables

Our balance control technique is also effective with the use of swing-COM RVs. The fact that significantly different choices of RV can be used successfully with otherwise identical control serves to illustrate that the proposed control approach is reasonably general.

Figure 4.8 shows a representative set of RV trajectory plots for the swing-COM vector trials. The plots indicate the trajectories of both feet through the whole cycle since the swing leg, and hence the swing-COM RV, changes legs each step. In contrast with the similar up-vector trajectories of Figure 4.2, the swing-COM-based RV trajectories do not exhibit "strong" limit cycle behaviour, but rather tends to drift around in near-cycles and/or converge very slowly onto a limit cycle if at all.

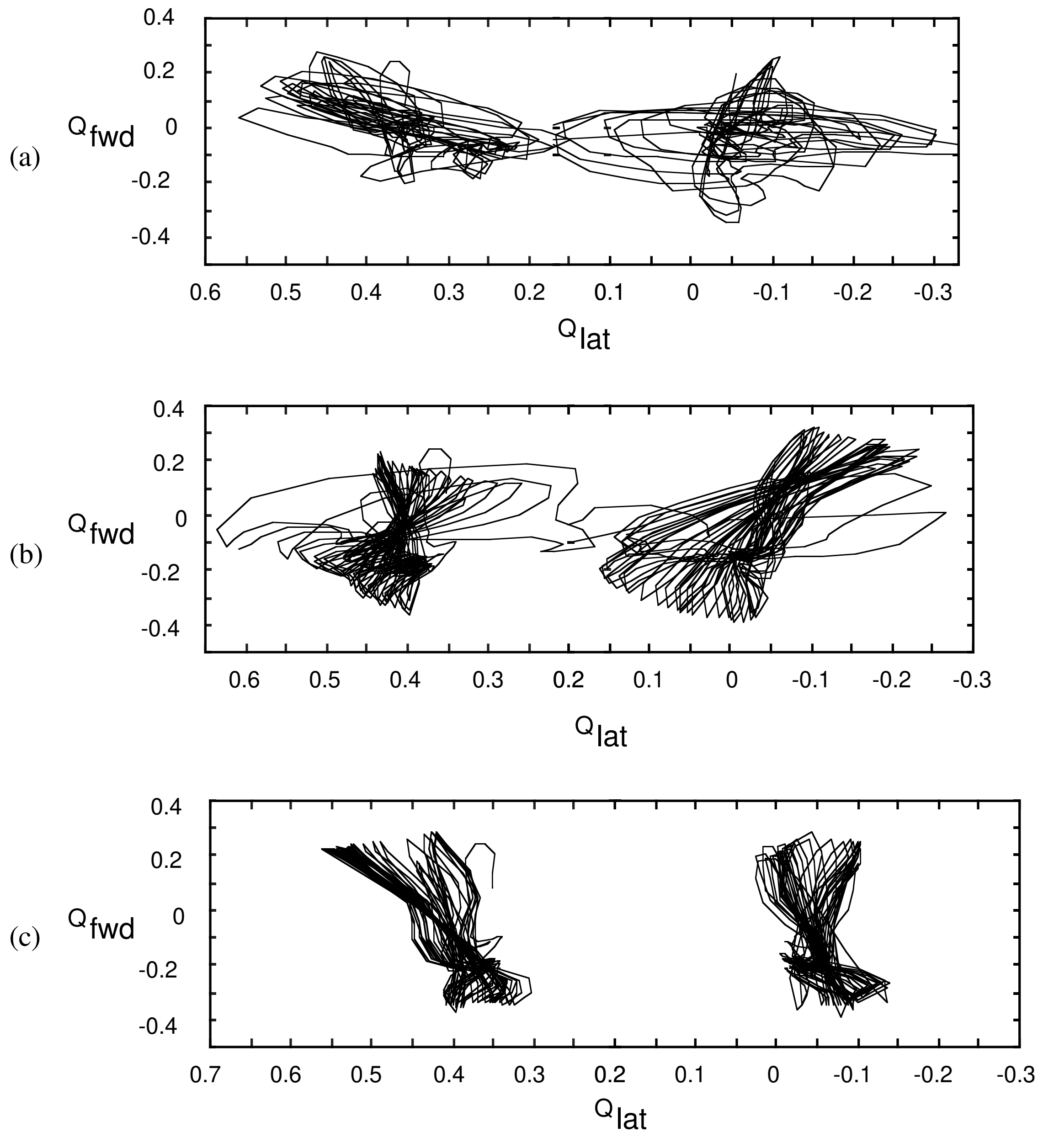

Figure 4.8 Continuous-time swing-COM RV phase diagrams. The two curves represent the left and right feet respectively (i.e. swing-COM and stance-COM at various times in the cycle).

(a) F-L-sampling, $Q^d = [-0.05,0]$

(b) L-F-sampling, $Q^d = [0,0]$

(c) SP-sampling, $Q^d = [0,0]$

Figure 4.9 shows the nominal range plots and hip plots for a series of trials using swing-COM RVs and stance hip control perturbations with each of the three sampling strategies (F-L, L-F and SP). The trials explore the useful range of the forward component of Q^d, with uniform sampling. The lateral component of Q^d is fixed at 0.0 for all trials. Torso servoing is not applied. All trials are a maximum of 60 steps long.

A few of observations can be made based on Figure 4.9 and on the corresponding animated motion:

1. The swing-COM RVs generate walking motions generally similar in nature to those generated using up-vector RVs. As with the up-vector results, there is a "nominal range" of Q^d values which produce the most successful walks.
2. In contrast to the up vector case, different sampling strategies give significantly different results. SP sampling generates the most stable motions and F-L sampling the least stable.
3. Unlike the up vector walks, which generally move straight forward, many swing-COM walks demonstrate a tendency of the biped to twist sideways about its own vertical axis. This tendency is most prevalent when using the F-L sampling strategy and is almost entirely absent for the SP sampling strategy.

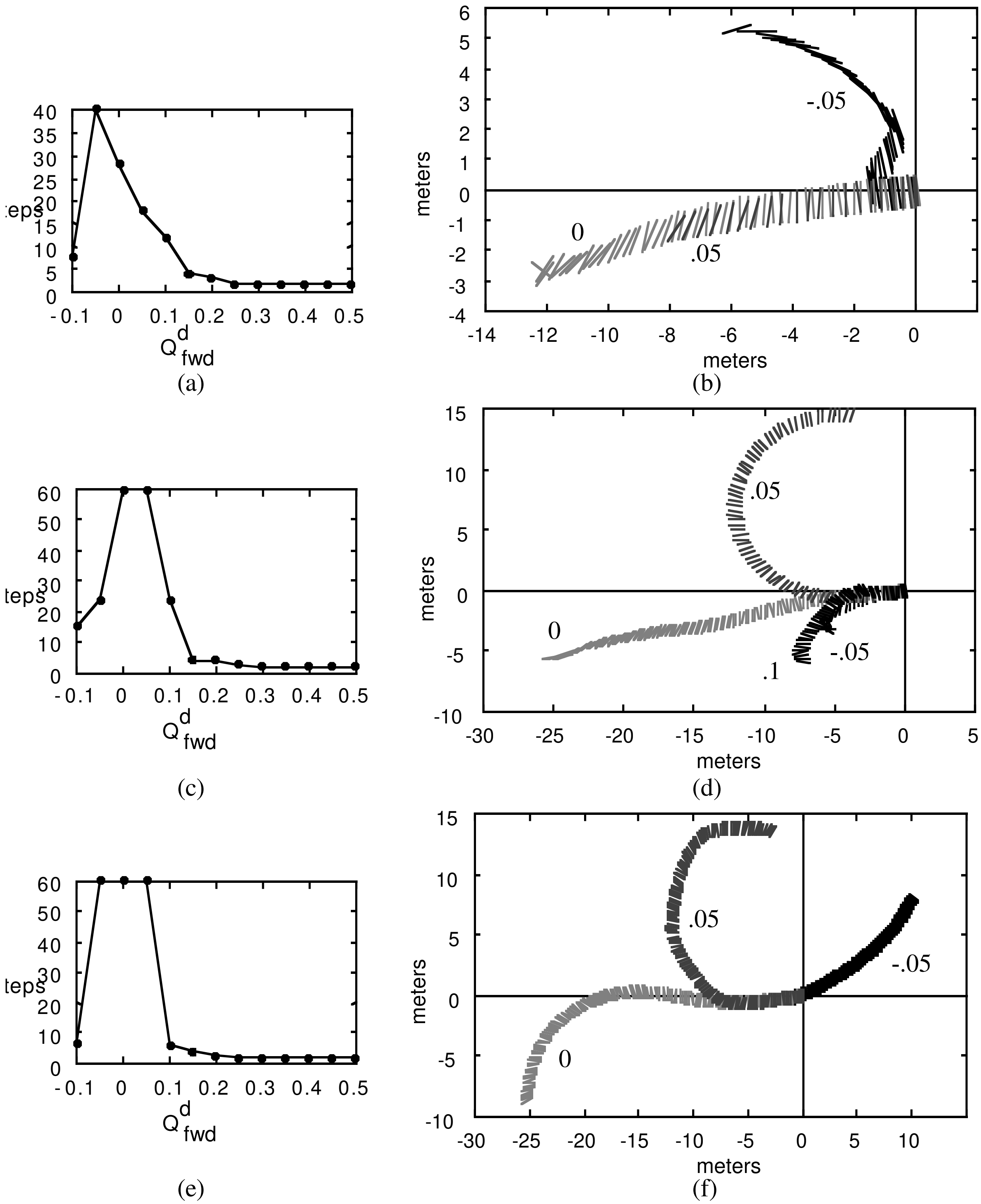

Figure 4.9 - Nominal swing-COM Q^d range and corresponding hip plots for each sampling method. Lateral $Q^d = 0.0$ for all trials. The biped initially faces left (i.e. in the -x direction).
(a) - (b) F-L sampling
(c) - (d) L-F sampling
(e) - (f) SP sampling

Figure 4.10 and Figure 4.11 show discrete RV value plots typical of the results obtained using swing-COM RVs. Q^d is indicated by a dotted line.

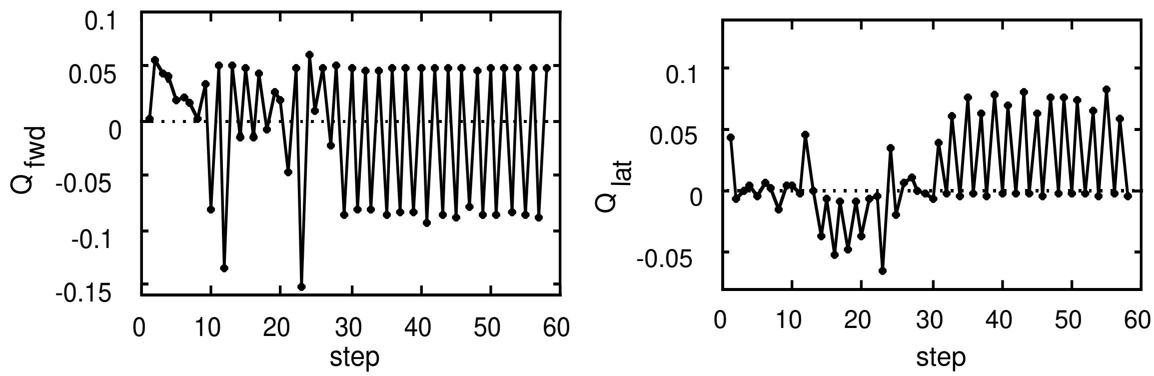

(a) forward component (b) lateral component

Figure 4.10 - Discrete RV values, Q_i^*, for L-F sampling, $Q^d = [0.05,0]$

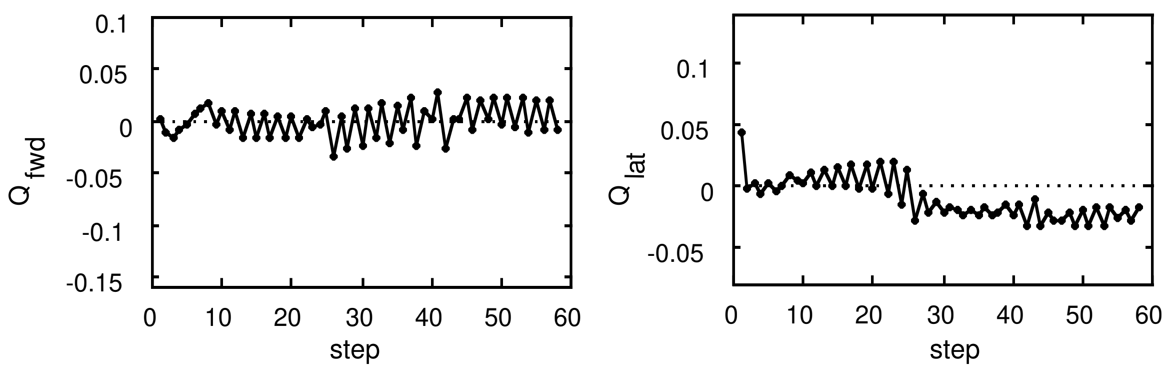

(a) forward component (b) lateral component

Figure 4.11 - Discrete RV values, Q_i^*, for SP sampling, $Q^d = [0.0,0]$

Overall, the results are not as good as those obtained with the up-vector RV. The swing-COM Q_i^* values are, in general, less stable, fall farther from their desired values with larger, more chaotic oscillations, and demonstrate a tendency to drift. Correspondingly, the continuous motion of the biped in most swing-COM trials is farther from a true limit cycle, qualitatively speaking.

Two particular problems are apparent when viewing the generated motion:

1. All three sampling strategies generate walks with step lengths which vary widely from one step to the next as shown in Figure 4.12. This contrasts sharply with the uniform step lengths generated when using up vector RVs.
2. "Tightrope" walking, similar to that present in some up vector-based walks, is also prevalent in the swing-COM trials. The use of swing-COM RVs, however, makes a reasonable solution possible by choosing Q^d with this problem in mind.

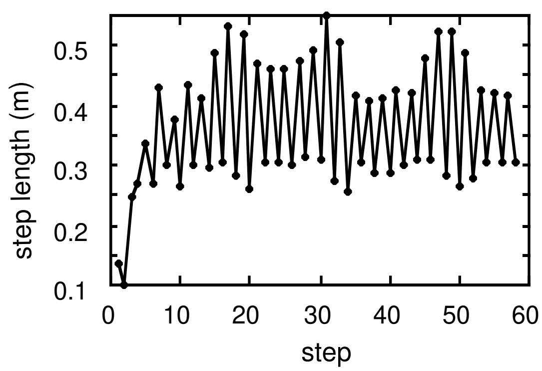

Figure 4.12 - Step length vs step number, SP sampling, Q^d = [0.05,0]

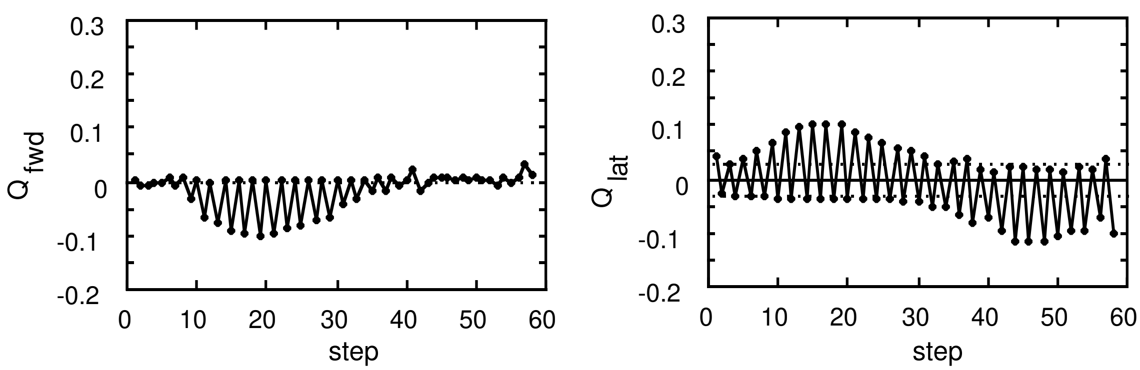

(a) forward component (b) lateral component

Figure 4.13 - Discrete RV values for SP sampling, Q^d = [0.0,±0.03]. Compare with Figure 4.11. Larger lateral step-to-step variation means less tightrope walking.

The first problem will be addressed in the next chapter. To solve the second problem, the lateral component of Q^d is chosen to give the swing foot a displacement slightly away from the body and the COM in the lateral dimension. Figure 4.13 shows the resulting Q_i^* for such an attempt based on the walk of Figure 4.11, which exhibits tightrope walking. A lateral Q^d component of ±0.03 is used instead of 0.0. The sign of Q^d is such that foot placement target is away from the COM. The resulting walk does not fall and exhibits much more realistic lateral foot placement.

4.3 Stance-COM Regulation Variables

While using the up-vector and swing-COM RVs achieves reasonable success in generating walking motions, similar use of the stance-COM RVs does not. Most trials fall during the second controlled step. The failures are due to the fact that even modest changes in the stance-COM RVs require very large stance hip perturbations which cause very large changes in the biped's state. Figure 4.14 illustrates this idea. Because of this result, the chosen balance parameters fail to reach a suitable state from which to begin the next cycle, even though the desired RV value might be attained.

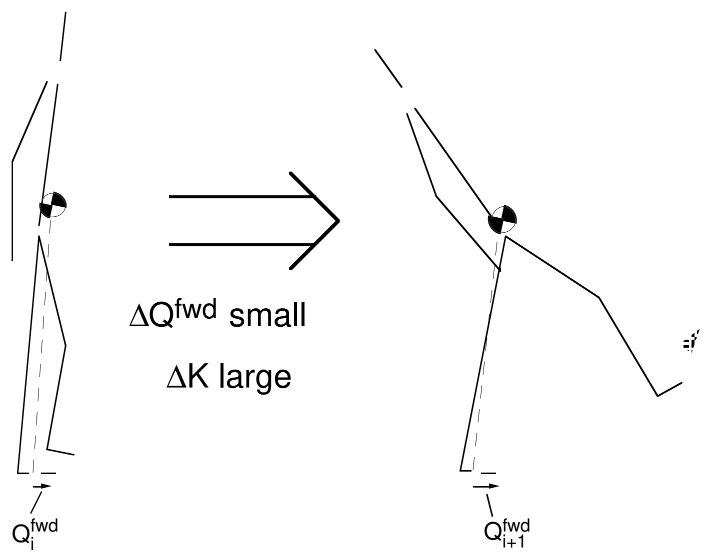

Figure 4.14 - Variation of stance-COM RV with stance hip pitch (ΔK)

While the walks all fall quickly, two interesting observations can be made:

1. The first controlled step reaches Q^d with a high degree of accuracy, i.e. the discrete system model of the first step is accurate.

2. The above holds for final perturbation scalings, K^*, far from the sample point scalings used to construct the linear discrete system model. That is, the model applies over a large change in state. Table 4.1 shows this for a number of desired values of Q^d. At one extreme, the model is still accurate for K^* as high as 13 times the sample scalings used to construct the model.

Taken together, these suggest the possibility of controlling non-trivial aperiodic motions in a similar way to the periodic motions of this thesis. Such motions would typically require a much larger controllable range of Q than cyclic motions since they typically involve a larger change from initial state to final state. An example of such an aperiodic motion would be standing up from sitting in a chair.

Q^d_{fwd}	Q^d_{lat}	K^*_{fwd}	K^*_{lat}	Q^*_{fwd}	Q^*_{lat}
.1	0	−36.318	+5.544	0.072	+0.007
.15	0	−10.918	+7.823	0.154	+0.030
.2	0	+14.481	+14.603	0.208	−0.001
.25	0	+39.881	−45.124	0.254	−0.015
.3	0	+65.280	−9.943	0.335	−0.003

Table 4.1 - Results of first controlled step using stance-COM RVs. K^*_{fwd} and K^*_{lat} are final stance hip perturbation scalings in degrees. Sample scalings for construction of linear models are $[K_{fwd},K_{lat}] = [\pm 5,\pm 1]$ (compare to K^*_{fwd} and K^*_{lat} in table).

Finally, because the particular choice of perturbation is the primary cause of the poor stability results with the stance-COM, it is quite possible that a better choice of perturbations might give better results. Using a stance ankle pitch perturbation to vary the force with which the stance foot pushes off the ground is one possible example.

4.4 Torso Servoing

All of the walks presented thus far suffer from an unaesthetic "bobbing" of the torso. This can be readily observed in the continuous-time RV phase diagrams such as those in Figure 4.2. Excursions in torso pitch of around 12 degrees are typical and they are quite apparent when watching animations of the balanced walks. While these motions may in fact be desirable in some cases, they tend to adversely affect the perceived quality of the motion when a realistic, natural looking walk is the eventual goal.

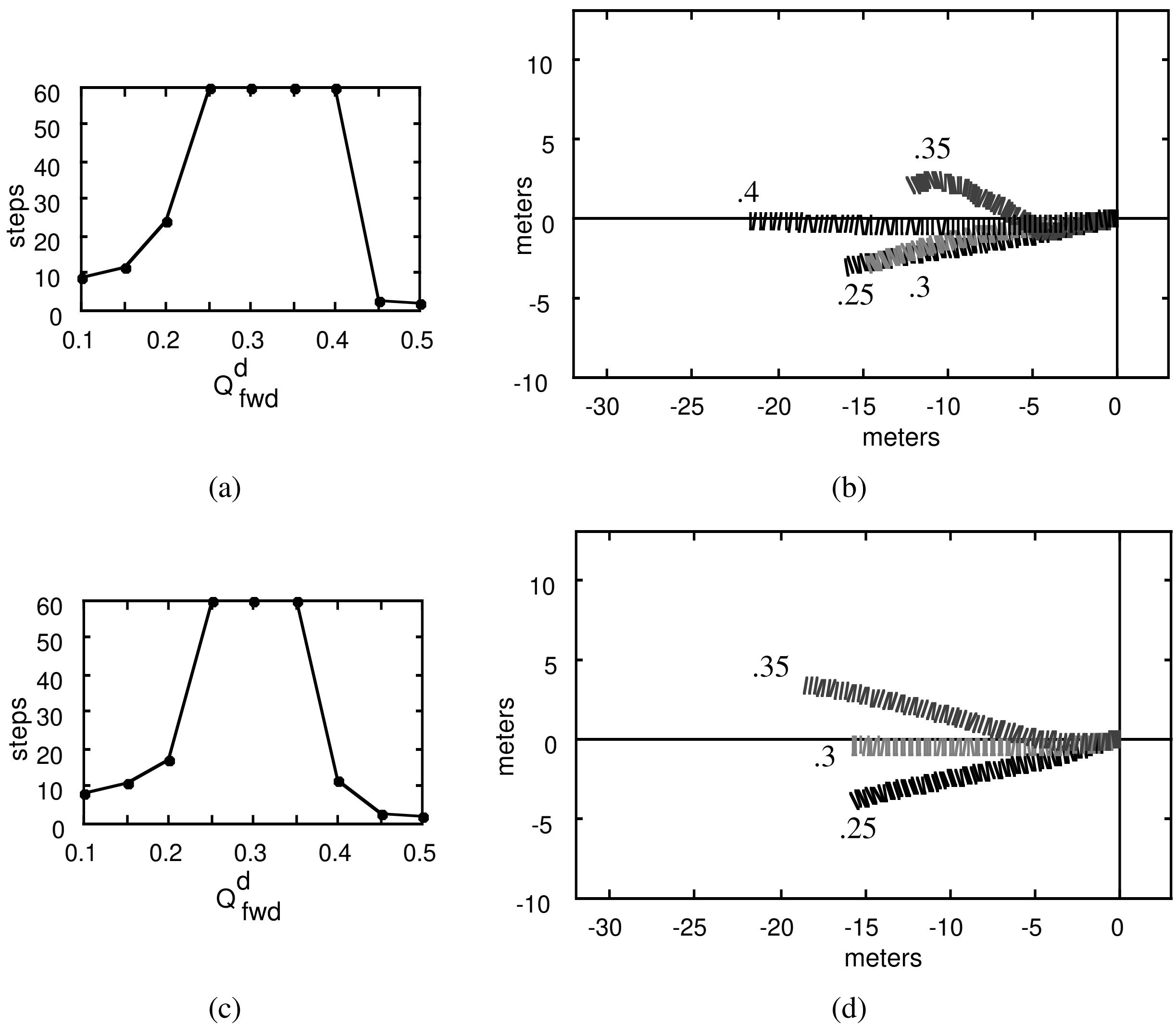

Figure 4.15 - Trial results based on the walks of Figure 4.3 with the addition of torso servoing to 5 degrees from world vertical. The biped initially faces left (i.e. in the -x direction).
(a) - (b) F-L sampling
(c) - (d) L-F sampling

Torso servoing significantly reduces the magnitude of the excursions in the forward dimension and, as a side effect, can also reduce the excursions in the lateral dimension. Figure 4.15 shows the results for a set of trials which use the same balance control parameters as the walks of Figure 4.3. In this set of trials, torso servoing is applied using a desired angle of 5 degrees forward from vertical.

The resulting paths are straighter and generally more consistent in direction than the non-torso servoed results. The useful range of Q^d increases in general. The phase diagram in Figure 4.16 illustrates the effectiveness of torso servoing at reducing the bobbing effect caused by the particular stance hip perturbation used. In this trial, torso servoing reduces the range of torso pitch from approximately 12 degrees to 3 degrees.

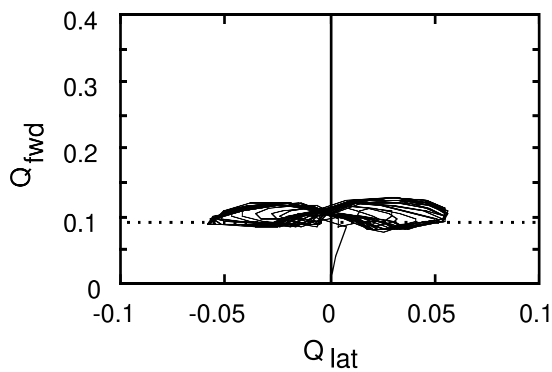

Figure 4.16 - Continuous-time up vector component phase diagram for human model with torso servoing to +5 degrees from world vertical ($Q_{servo} \approx .09$). Compare to Figure 4.2.

4.5 Robo-bird Running

Figure 4.17 shows the base PCG used to generate a running motion for the robo-bird model, shown in Figure 4.18. While the base PCG differs from that used for the human model, it is balanced using up-vector RVs and stance hip pitch and roll perturbations as with the human model.

DOF:		1	2:0	2:1	3	4	5	6:0	6:1	7:0	7:1	8	9	10	11:0	11:1	transition info
	S1	0	0	0	80	-95	45	-45	0	0	15	55	-65	25	-25	0	0.1
state	S2	0	0	0	80	-95	45	-45	0	0	15	55	-65	25	-25	0	0.1
	S3	0	0	15	55	-65	25	-25	0	0	0	80	-95	45	-45	0	0.1
	S4	0	0	15	55	-65	25	-25	0	0	0	80	-95	45	-45	0	0.1

Figure 4.17 - Robo-bird base PCG for running

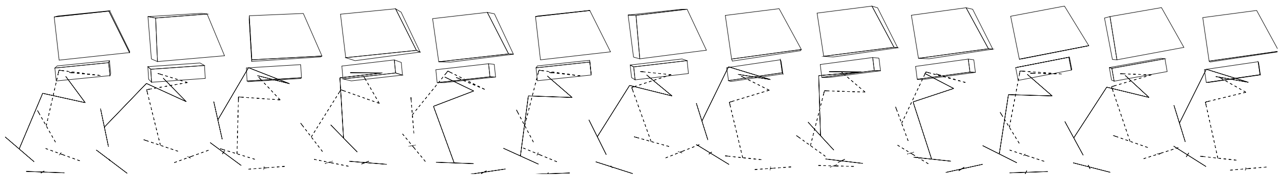

Figure 4.18 - A running robo-bird

While both the robo-bird and human models are bipeds, their dynamics are different. When standing and walking, the human model is supported by the rigidity of its straight stance leg, which typically has little or no freedom in the vertical direction. In theory, no actuator forces are required to prevent the human model from collapsing. The leg structure of the robo-bird model is such that actuator forces must constantly be applied even to remain standing upright. This means there is a significant amount of vertical compliance when moving, leading to “bouncy” motions. As well, the base of the robo-bird model is wide enough to make standing on one foot for any length of time difficult. These factors make a dynamic running motion more natural than a walk for this model.

4.6 Conclusions

In this chapter we have presented evidence that the discrete limit cycle control technique introduced in Chapter 3 can be used to generate balanced walking motions for the human model and a running motion for the robo-bird model. Two choices of RV, based on the up-vector and the swing-COM vector, were successfully applied to this end. A torso servo was shown to be useful in improving the aesthetics of the human model’s motion. Finally, a running motion for the robo-bird motion was used to demonstrate the applicability of the control technique to a different motion and model. In the next chapter, we will present a number of interesting gait variations, all of which make use of the same basic form of balance control demonstrated here.